

Imaging polarimetry of forest canopies: how the azimuth direction of the sun, occluded by vegetation, can be assessed from the polarization pattern of the sunlit foliage

Ramón Hegedüs,¹ András Barta,¹ Balázs Bernáth,² Victor Benno Meyer-Rochow,^{3,4}
and Gábor Horváth^{1,*}

¹Department of Biological Physics, Bio-optics Laboratory, Physical Institute, Eötvös University, H-1117 Budapest, Pázmány sétány 1, Hungary

²Department of Zoology, Plant Protection Institute of the Hungarian Academy of Sciences, H-1525 Budapest, P. O. B. 102, Hungary

³Jacobs University (formerly International University Bremen), Campus Ring 6, D-28759 Bremen, Germany

⁴Department of Biology, University of Oulu, SF-90014, Oulu, Finland

*Corresponding author: gh@arago.elte.hu

Received 8 March 2007; accepted 23 April 2007;
posted 30 April 2007 (Doc. ID 80856); published 9 August 2007

Radiance, color, and polarization of the light in forests combine to create complex optical patterns. Earlier sporadic polarimetric studies in forests were limited by the narrow fields of view of the polarimeters used in such studies. Since polarization patterns in the entire upper hemisphere of the visual environment of forests could be important for forest-inhabiting animals that make use of linearly polarized light for orientation, we measured 180° field-of-view polarization distributions in Finnish forests. From a hot air balloon we also measured the polarization patterns of Hungarian grasslands lit by the rising sun. We found that the pattern of the angle of polarization α of sunlit grasslands and sunlit tree canopies was qualitatively the same as that of the sky. We show here that contrary to an earlier assumption, the α -pattern characteristic of the sky always remains visible underneath overhead vegetation, independently of the solar elevation and the sky conditions (clear or partly cloudy with visible sun's disc), provided the foliage is sunlit and not only when large patches of the clear sky are visible through the vegetation. Since the mirror symmetry axis of the α -pattern of the sunlit foliage is the solar-antisolar meridian, the azimuth direction of the sun, occluded by vegetation, can be assessed in forests from this polarization pattern. Possible consequences of this robust polarization feature of the optical environment in forests are briefly discussed with regard to polarization-based animal navigation. © 2007 Optical Society of America

OCIS codes: 010.1290, 110.2960, 120.5410, 280.1310, 330.7310.

1. Introduction

Polarimetric remote sensing has numerous applications in the field of agriculture [1] and many of the methods used exploit information about polarized light reflected from vegetation [2]. The polarization signature of vegetated surfaces can be used to distinguish different types of crops and to indicate developmental states and possible stress factors (e.g. water deficiency,

disease, excessive salinity) that could affect production [2]. Earlier, polarization characteristics of plant surfaces were measured only by point-source polarimetry [1,3,4–9], but then imaging polarimetry became available to investigate reflection-polarization characteristics of plant surfaces [10,11]. Compared with the polarimetric remote sensing of vegetation from above, i.e., from aircrafts or satellites, the polarimetric study of forest foliage from beneath the tree canopy has been a rather neglected subject of research.

The optical environment in forests presents complex spatial distributions of light radiance and color [12] and the polarized light field is equally complex.

In one set of preliminary measurements, Brines and Gould [3] pointed their polarimeter at a shaded-tree and found that the direction of polarization in the ultraviolet (UV) spectral range was less than 5° from the value predicted by the single-scattering Rayleigh model, while in the green and red parts of the spectrum the errors were 97° , and 92° , respectively. Based on this observation, they hypothesized that under certain circumstances biologically significant Rayleigh polarization patterns may exist against overhead vegetation at UV wavelengths. Using videopolarimetry, Shashar *et al.* [10] studied the linear polarization of light in a Venezuelan tropical rain forest. They found that the celestial polarization pattern remains visible underneath the forest canopy, provided patches of clear sky are visible through the overhead vegetation. They characterized some distinct light environments in the forest, each having a typical linearly polarized light field. They concluded that polarization-based animal navigation would be limited to spaces exposed to several extended portions of the clear sky, and that other forms of orientation throughout the forest would include the remote sensing of surface features, object detection, and camouflage violations.

Apart from the pioneering studies by Brines and Gould [3] and Shashar *et al.* [10], polarization characteristics of the light environment of forests and forest edges have not been investigated. Since Brines and Gould [3] measured the polarization of light reflected by, or passing through leaves only at a single point of a tree, and the field of view of the videopolarimeter of Shashar *et al.* [10], was relatively small (some tens of degrees both horizontally and vertically), the polarization patterns of the entire upper hemisphere of the visual environment in forests could not have been investigated. However, the complete pattern may be important for certain forest animals using polarization-based means of orientation. Thus, using full-sky imaging polarimetry, we measured the 180° field-of-view polarization patterns of the overhead foliage in a variety of forest types in Finland. From a hot air balloon we also measured the polarization patterns of Hungarian grasslands lit by the rising sun. In this work we document that the pattern of the angle of polarization of the upwelling light from sunlit grasslands and that of the downwelling light from sunlit tree canopies are qualitatively the same as that of the sky, independently of the solar elevation and the sky conditions. Possible consequences of this finding on polarization-based animal navigation in forests are briefly discussed.

2. Materials and Methods

The polarization patterns of grasslands lit by the sun 30–35 minutes after sunrise, when the solar elevation angle above the horizon was 4.5° , were measured in calm weather from a hot air balloon belonging to the Hungarian Airlines Aero Club (MALEV, Budapest) at heights of 100–200 meters above ground. The flight took place on August 25, 2001 with a crew

consisting of Attila Bakos (pilot), András Barta, Balázs Bernáth, and Gábor Horváth. The balloon was launched prior to the local sunrise (at 05:56 = local summer time = UTC + 2) from the immediate vicinity of the Hungarian town of Pákozd ($47^\circ 13' N$, $18^\circ 33' E$). During the flight the atmosphere was slightly hazy but cloudless, the rising sun was not occluded by distant clouds. The ground surface was covered by green grass. Further details of this measurement were described elsewhere [13].

The polarization patterns of skies and tree canopies were measured near the outskirts of the Finnish town of Oulu ($65^\circ 0' N$, $25^\circ 26' E$) between 10 and 19 August 2006. Since during the measurements the weather was calm, the leaves of the foliage were motionless. The date, time (local summer time = UTC + 3), solar elevation, and sky conditions during the measurements are summarized in Table 1. The solar elevation angle ε from the horizon was determined by the exact time and geographical coordinates of the place of measurements using the online solar position calculator of the U. S. Naval Observatory, Astronomical Applications Department (<http://aa.usno.navy.mil>).

The polarization patterns of the grassland, sky, and overhead vegetation were measured by full-sky imaging polarimetry, which was described by Gál *et al.* [14]. A 180° field of view was ensured by a Nikon-Nikkor fisheye lens ($F = 2.8$, focal length = 8 mm) with a built-in rotating disc with three mounted broadband (275–750 nm) neutral density linearly polarizing filters (Polaroid HNP'B) with three different polarization axes (0° , 45° , and 90° from the radius of the disc). The detector was the photo emulsion of a Kodak Elite Chrome ED 200 ASA color reversal film (with spectral maxima and half-bandwidths of $\lambda_{\text{red}} = 650 \pm 40$ nm, $\lambda_{\text{green}} = 550 \pm 40$ nm, $\lambda_{\text{blue}} = 450 \pm 40$ nm) in a photographic camera (Nikon F801). For a given scene, three photographs were taken for the three different directions of the transmission axis of the polarizers. The camera was set on a tripod so that the optical axis of the fisheye lens was vertical and pointed either toward the zenith (for skies and overhead vegetation) or to the nadir (for grasslands). After 24-bit (3×8 for red, green, and blue) digitization (by a Canon Arcus 1200 scanner) of the three chemically developed color pictures for a given scene and their computer evaluation, patterns of the radiance I , the degree of linear polarization p , and the angle of polarization α of light were determined as color-coded, two-dimensional, circular maps, in which the center was the zenith/nadir, the perimeter the horizon, and the zenith/nadir angle θ proportional to the radius measured from the zenith/nadir (zenith/nadir: $\theta = 0^\circ$, horizon: $\theta = 90^\circ$; our fisheye mapping had an approximately equisolid angle). These patterns were obtained in the red, green, and blue spectral ranges, in which the three color-sensitive layers of the photo emulsion used have maximal sensitivity. The values of p and α were measured by our polarimeter with an accuracy of $\Delta p = \pm 1\%$ and $\Delta \alpha = \pm 2^\circ$, respectively.

Table 1. Date, Time, Solar Elevation Angle ε , Sky and Canopy Conditions During our Polarimetric Measurements Performed in Hungary (Scene S0) and Finland (Scenes S1–S43)

Scene Number	Date	Time	ε	Sky and Canopy Conditions	
Hungarian town Pákozd (47° 13' N, 18° 33' E)					
S0	25 August 2001	06:30 (UTC+2)	$\varepsilon = 4.5^\circ$	Sunrise, Sunlit Grassland, Clear Sky	
Finnish town Oulu (65° 0' N, 25° 26' E)					
S1	10 August 2006	20:00 (UTC+3)	$\varepsilon = 10.3^\circ$	Sunset, Sunlit Birch Trees, Cloudy Sky	
S2		20:05	$\varepsilon = 9.8^\circ$	Sunset, Sunlit Birch & Pine Trees, Clear Sky	
S3	11 August 2006	20:10	$\varepsilon = 9.3^\circ$	Sunset, Sunlit Poplar Trees, Cloudy Sky	
S4		20:18	$\varepsilon = 8.5^\circ$	Sunset, Clear Sky	
S5		21:25	$\varepsilon = 2.3^\circ$	Sunset, Sunlit Poplar Trees, Cloudy Sky	
S6		21:30	$\varepsilon = 1.9^\circ$	Sunset, Clear Sky	
S7		19:45	$\varepsilon = 11.5^\circ$	Sunset, Sunlit Poplar Trees, Cloudy Sky	
S8		19:50	$\varepsilon = 11.0^\circ$	Sunset, Clear Sky	
S9	12 August 2006	20:58	$\varepsilon = 4.4^\circ$	Sunset, Clear Sky	
S10		21:05	$\varepsilon = 3.7^\circ$	Sunset, Sunlit Poplar Trees, Cloudy Sky	
S11		21:15	$\varepsilon = 2.9^\circ$	Sunset, Sunlit Birch Trees, Cloudy Sky	
S12		19:55	$\varepsilon = 10.2^\circ$	Sunset, Sunlit Pine Trees, Cloudy Sky	
S13		20:00	$\varepsilon = 9.7^\circ$	Sunset, Sunlit Pine Trees, Cloudy Sky	
S14		20:05	$\varepsilon = 9.2^\circ$	Sunset, Cloudy Sky	
S15		21:00	$\varepsilon = 3.9^\circ$	Sunset, Cloudy Sky	
S16		21:05	$\varepsilon = 3.5^\circ$	Sunset, Sunlit Pine Trees, Cloudy Sky	
S17		21:05	$\varepsilon = 3.5^\circ$	Sunset, Sunlit Pine Trees, Cloudy Sky	
S18		13 August 2006	20:50	$\varepsilon = 4.6^\circ$	Sunset, Sunlit Birch trees, Cloudy Sky
S19			20:55	$\varepsilon = 4.1^\circ$	Sunset, Cloudy Sky
S20			21:18	$\varepsilon = 2.1^\circ$	Sunset, Sunlit Birch Trees, Cloudy Sky
S21	21:24		$\varepsilon = 1.6^\circ$	Sunset, Cloudy Sky	
S22	14 August 2006	21:12	$\varepsilon = 2.3^\circ$	Sunset, Sunlit Birch Trees, Cloudy Sky	
S23		21:20	$\varepsilon = 1.6^\circ$	Sunset, Cloudy Sky	
S24	15 August 2006	20:13	$\varepsilon = 7.5^\circ$	Sunset, Sunlit Pine Trees, Cloudy Sky	
S25		20:18	$\varepsilon = 7.0^\circ$	Sunset, Sunlit Pine Trees, Cloudy Sky	
S26		20:24	$\varepsilon = 6.4^\circ$	Sunset, Cloudy Sky	
S27		20:41	$\varepsilon = 4.8^\circ$	Sunset, Poplar Trees, Cloudy Sky, Occluded Sun	
S28		20:48	$\varepsilon = 4.1^\circ$	Sunset, Sunlit Birch Trees, Cloudy Sky	
S29		20:53	$\varepsilon = 3.7^\circ$	Sunset, Overcast Sky	
S30		17 August 2006	12:00	$\varepsilon = 36.5^\circ$	Noon, Pine Trees, Overcast Sky, Occluded Sun
S31	12:10		$\varepsilon = 37.0^\circ$	Noon, Overcast Sky	
S32	12:16		$\varepsilon = 37.2^\circ$	Noon, Poplar Trees, Overcast Sky, Occluded Sun	
S33	18 August 2006		12:15	$\varepsilon = 36.8^\circ$	Noon, Sunlit Poplar Trees, Cloudy Sky
S34		12:31	$\varepsilon = 37.3^\circ$	Noon, Sunlit Pine Trees, Cloudy Sky	
S35		12:49	$\varepsilon = 37.8^\circ$	Noon, Sunlit Birch Trees, Cloudy Sky	
S36		12:54	$\varepsilon = 37.9^\circ$	Noon, Clear Sky	
S37		12:58	$\varepsilon = 37.9^\circ$	Noon, Sunlit Pine Trees, Cloudy Sky	
S38		13:19	$\varepsilon = 38.1^\circ$	Noon, Sunlit Pine Trees, Cloudy Sky	
S39		19 August 2006	14:51	$\varepsilon = 35.6^\circ$	Afternoon, Sunlit Birch Trees, Cloudy Sky
S40	15:02		$\varepsilon = 35.0^\circ$	Afternoon, Clear Sky	
S41	15:55		$\varepsilon = 31.6^\circ$	Afternoon, Sunlit Pine Trees, Cloudy Sky	
S42	19:45		$\varepsilon = 9.1^\circ$	Sunset, Sunlit Birch Trees, Cloudy Sky	
S43	20:00		$\varepsilon = 7.6^\circ$	Sunset, Clear Sky	

The noisiness n of a given α -pattern (Table 2) was calculated in the following way: The α -pattern was scanned throughout with a 5-pixel \times 5-pixel window, in which the standard variance (σ^2) of α was calculated, and then the average of the standard variances of all 5-pixel \times 5-pixel windows was obtained. Finally, this value was normalized to that of white noise calculated with the same method. Thus, noisiness n of an α -pattern denotes how noisy it is com-

pared with the white noise ($n = 0\%$: no noise, $n = 100\%$: white noise).

The foliage ratio f , giving the percentage of vegetation in the celestial hemisphere [Fig. 3(B), Table 2], was determined by creating a two-colored mask of the photographs consisting of regions of sky and overhead vegetation using the selective color filter of the Adobe Photoshop software. Typical colors of the vegetation (green, yellow, brown) were trans-

Table 2. Optical Characteristics of the Hungarian (S0) and Finnish (S1–S43) Scenes Measured in the Red (R, 650 nm), Green (G, 550 nm), and Blue (B, 450 nm) Parts of the Spectrum and Averaged over the Entire Hemispherical Field of View. The Definition of Noisiness n of α Is Given in the Materials and Methods Section. The Foliage Ratio f Gives the Percentage of the Overhead Vegetation of the Full Celestial Hemisphere (Not Applicable in Scenes with Open Skies). The Date, Time, Latitude, Longitude, Solar Elevation and Sky Conditions of Scenes S0–S43 are Given in Table 1

Scene Number	Figure Number	Degree of Linear Polarization p (%)			Noisiness n (%) of α			Foliage Ratio f (%)
		R	G	B	R	G	B	
S0	Fig. 2	9 ± 6	6 ± 4	7 ± 4	16	11	13	–
S1	Fig. 4/S1	19 ± 14	19 ± 15	20 ± 16	27	26	25	66.7%
S2	Fig. 4/S2	21 ± 15	19 ± 14	19 ± 15	24	24	22	68.6%
S3	Fig. 4/S3	19 ± 13	19 ± 13	19 ± 14	27	26	23	60.8%
S4	Fig. 4/S4	28 ± 20	23 ± 17	20 ± 15	4	4	6	–
S5	Fig. 4/S5	15 ± 11	17 ± 13	20 ± 15	26	24	23	72.6%
S6	Fig. 4/S6	23 ± 13	21 ± 12	15 ± 10	4	4	4	–
S7	Fig. 4/S7	17 ± 11	17 ± 12	20 ± 15	34	34	33	75.4%
S8	Fig. 4/S8	26 ± 18	22 ± 16	20 ± 15	5	5	7	–
S9	Fig. 4/S9	29 ± 21	27 ± 20	26 ± 19	6	5	6	–
S10	Fig. 4/S10	20 ± 15	21 ± 16	24 ± 19	23	23	24	75.4%
S11	Fig. 4/S11	12 ± 9	15 ± 11	16 ± 13	40	45	46	67.7%
S12	Fig. 4/S12	16 ± 13	16 ± 13	17 ± 15	34	35	36	66.7%
S13	Fig. 4/S13	16 ± 12	18 ± 13	18 ± 14	35	40	40	74.9%
S14	Fig. 4/S14	11 ± 10	11 ± 9	10 ± 9	19	17	12	–
S15	Fig. 4/S15	27 ± 19	25 ± 17	24 ± 16	7	5	4	–
S16	Fig. 4/S16	17 ± 12	19 ± 13	20 ± 14	19	19	20	63.8%
S17	Fig. 4/S17	22 ± 16	23 ± 16	24 ± 17	21	22	24	72.5%
S18	Fig. 4/S18	11 ± 11	13 ± 13	15 ± 14	32	30	31	65.2%
S19	Fig. 4/S19	10 ± 8	12 ± 8	12 ± 8	9	8	8	–
S20	Fig. 4/S20	16 ± 12	18 ± 14	20 ± 15	31	34	36	79.2%
S21	Fig. 4/S21	14 ± 9	15 ± 10	16 ± 10	7	7	7	–
S22	Figs. 3, 4/S22	21 ± 14	21 ± 14	23 ± 16	45	43	41	84.8%
S23	Fig. 4/S23	16 ± 10	17 ± 10	16 ± 10	6	5	5	–
S24	Fig. 4/S24	12 ± 10	14 ± 12	13 ± 11	46	45	45	62.7%
S25	Fig. 4/S25	15 ± 12	16 ± 13	16 ± 13	46	47	47	73.2%
S26	Fig. 4/S26	9 ± 8	10 ± 7	10 ± 6	21	13	7	–
S27	Fig. 4/S27	17 ± 14	19 ± 15	19 ± 15	41	42	42	79.9%
S28	Fig. 4/S28	15 ± 11	16 ± 12	17 ± 13	50	51	50	77.5%
S29	Fig. 4/S29	7 ± 5	7 ± 6	7 ± 6	20	17	14	–
S30	Fig. 4/S30	12 ± 11	12 ± 12	13 ± 13	37	38	40	64.5%
S31	Fig. 4/S31	6 ± 6	6 ± 6	5 ± 7	31	35	35	–
S32	Fig. 4/S32	18 ± 15	18 ± 16	19 ± 16	40	40	43	79.5%
S33	Fig. 4/S33	21 ± 16	20 ± 16	20 ± 17	34	34	35	75.6%
S34	Fig. 4/S34	15 ± 11	15 ± 12	16 ± 13	46	47	44	86.5%
S35	Fig. 4/S35	19 ± 12	19 ± 12	22 ± 14	35	38	37	82.1%
S36	Fig. 4/S36	23 ± 19	20 ± 14	18 ± 13	7	6	5	–
S37	Fig. 4/S37	19 ± 14	20 ± 15	22 ± 16	45	45	44	89.2%
S38	Fig. 4/S38	24 ± 16	22 ± 15	21 ± 16	26	25	25	68.3%
S39	Fig. 4/S39	17 ± 12	16 ± 11	21 ± 14	41	43	36	82.2%
S40	Fig. 4/S40	29 ± 23	23 ± 15	20 ± 13	7	5	4	–
S41	Fig. 4/S41	22 ± 14	21 ± 12	21 ± 12	29	27	24	68.7%
S42	Fig. 4/S42	18 ± 12	18 ± 12	19 ± 12	29	28	23	70.2%
S43	Fig. 1	26 ± 16	22 ± 13	16 ± 10	3	2	3	–

formed to black, and those of the open sky (blue, white, gray) to white. Using this manual filtering, the value of f could be measured with an error of about $\pm 1\%$.

The theoretical α -patterns of the clear sky in Fig. 6 were calculated on the basis of the single-scattering Rayleigh model [2] and the model of Berry *et al.* [15] based on the neutral points, later derived using multiple scattering by Hannay [16]. The latter model provides a very good quantitative approximation of

experimental clear sky α -patterns, particularly in respect to the existence of neutral points. The model has three parameters to be freely set: two for the sun position (solar elevation and azimuth angles) and one for the angular distance between the Brewster and the Babinet neutral points. In our case the theoretical α -patterns in Fig. 6 were computed according to the solar elevation angle calculated on the basis of the exact time and geographical coordinates of the site of measurement. The angle between the Brewster and

Babinet points was assumed to be 40° , as under normal conditions [2].

3. Results

Figure 1 shows the color photograph and the p - and α -patterns of a clear (cloudless, blue) sky (scene S43, Tables 1 and 2) measured in the red, green, and blue

parts of the spectrum. p of light from the clear sky was highest at approximately 90° from the sun and gradually decreased toward the solar and antisolar points [Fig. 1(B)–1(D)]. At a given point in the clear sky, p was highest in the red and lowest in the blue spectral range (Table 2). The α of light from the clear sky had a typical pattern [Fig. 1(E)–1(G)]: the isolines

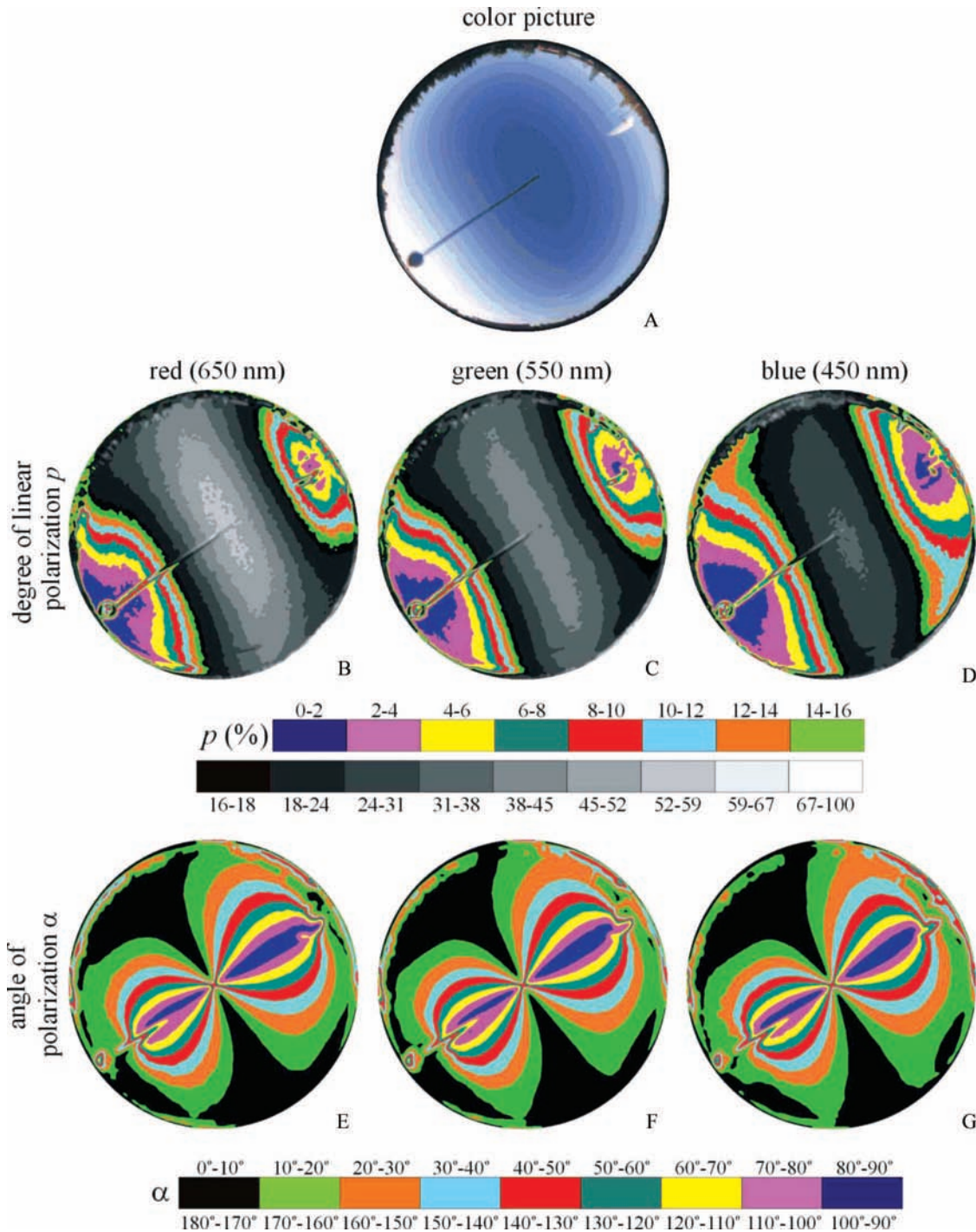


Fig. 1. (Color online) Color photograph (A), and patterns of the degree of linear polarization p (B–D) and the angle of polarization α from the local meridian (E–G) of a clear sky (scene S43, Tables 1 and 2), measured by 180° field-of-view imaging polarimetry in the red, green and blue parts of the spectrum. The optical axis of the fisheye lens was vertical, thus the horizon is the perimeter and the center of the circular patterns is the zenith. At the perimeter of the circular color picture the dark silhouette of trees can be seen. The sun near the horizon was occluded by a small black disc placed on a thin wire, which is seen radially in the circular patterns.

with $\alpha = \text{constant}$ were always 8-shaped with a cross-point at the zenith and an axis of mirror symmetry coinciding with the solar-antisolar meridian in such a way that the smaller loop of the figure-8 occurred consistently in the solar half of the sky. (We would like to emphasize that the crossing of the α -isolines at the zenith is purely a geometrical artifact and the consequence of the definition of α , rather than a true polarization singularity). In Figs. 1(E)–1(G) the different intervals of α are shaded by various colors (orange, for example, codes the intervals $20^\circ \leq \alpha \leq 30^\circ$ and $140^\circ \leq \alpha \leq 150^\circ$). In Figs. 1(E)–1(G) the typical figure-8 pattern of the area of each particular color is clearly seen. We measured the p - and α -patterns of some other clear skies (scenes S4, S6, S8, S9, S36, S40; Tables 1 and 2), and obtained always the same optical characteristics. Depending on the wavelength, solar elevation, and atmospheric turbidity, the maximum of p of light from the clear sky was $25\% \leq p_{\max}^{\text{clear}} \leq 65\%$, and the noisiness n of α of the clear sky was $2\% \leq n_{\text{clear}} \leq 7\%$ (Table 2, Fig. 1). If the sky was partly cloudy (scenes S14, S15, S19, S21, S23, S26) or overcast (scenes S29, S31), p_{\max} of cloudlight decreased considerably ($16\% \leq p_{\max}^{\text{cloudy}} \leq 27\%$; $12\% \leq p_{\max}^{\text{overcast}} \leq 13\%$), but the α -pattern remained qualitatively the same (apart from scene S31 with a very heavy overcast) as that of the clear sky. Depending on the degree of cloudiness and the wavelength, the noisiness n of α of partly cloudy and overcast skies was $5\% \leq n_{\text{cloudy}} \leq 21\%$ and $14\% \leq n_{\text{overcast}} \leq 35\%$ (Table 2). Hence, as the cloudiness increased, p of skylight decreased, the noisiness n of α increased, but the α -pattern remained qualitatively the same. These findings are corroborated by the earlier results of Hegedüs *et al.* [17–19].

Figure 2 features the color photograph and the p - and α -patterns of a grassland lit by the rising sun (scene S0, Tables 1 and 2), measured at an altitude of 100 meters from a hot air balloon in the red, green, and blue spectral ranges. p_{\max} of light reflected from the green grass was highest in the blue ($p_{\max}^{\text{blue}} = 15\%$) and lowest in the green ($p_{\max}^{\text{green}} = 10\%$). Depending on the wavelength, the noisiness n of α of the grass-reflected light ranged from 11% to 16%, which represents values that are much larger than those of the clear sky ($2\% \leq n_{\text{clear}} \leq 7\%$). Remarkably, the α -pattern of the sunlit grassland was qualitatively the same as that of the clear sky: the α -pattern was characterized by the typical figure-8 pattern, the mirror symmetry axis of which was the solar-antisolar meridian [Figs. 2(E)–2(G)]. We measured the polarization characteristics of some other sunlit grasslands from the hot air balloon and obtained similar results to those shown in Fig. 2 and Table 2.

Figure 3 shows the color photograph and the p - and α -patterns of the overhead vegetation in a forest composed of birch trees lit by the setting sun (scene S22, Tables 1 and 2) measured in the red, green, and blue parts of the spectrum. Figure 4 displays the α -patterns of numerous different skies and tree canopies (scenes S1–S42, Tables 1 and 2) measured in the blue spectral range. Quite similar α -patterns

were obtained in the green and red spectral ranges (not presented here). The foliage ratio f ranged from 60.8% to 89.2% (Table 2). Depending on the wavelength, the sky conditions and f , the maximum of p of light from the forest canopy was $21\% \leq p_{\max}^{\text{foliage}} \leq 43\%$ (Table 2), values that are smaller than those of the clear sky ($25\% \leq p_{\max}^{\text{clear}} \leq 65\%$). On the other hand, the noisiness n of the α -pattern of skies with overhead vegetation was $19\% \leq n_{\text{foliage}} \leq 51\%$; values being 7.2–9.5 times larger than those of the clear sky ($2\% \leq n_{\text{clear}} \leq 7\%$), but only 1.4–1.5 times larger than the n -values of overcast skies ($14\% \leq n_{\text{overcast}} \leq 35\%$).

Most remarkably, if the foliage was sunlit (scenes S1–S3, S5, S7, S10–S13, S16–S18, S20, S22, S24, S25, S28, S33–S35, S37–S39, S41, S42 in Fig. 4), the α -pattern of the overhead vegetation was qualitatively always the same as that of the clear sky: the α -isolines had the typical figure-8 pattern with a mirror symmetry axis along the solar-antisolar meridian, independently of the solar elevation and the sky conditions (clear or partly cloudy with visible sun's disc). However, beyond the increased noisiness n of tree canopies, there is another qualitative difference between the α -patterns of the sunlit overhead vegetation and the clear sky: under the same sky conditions the 8-shaped α -isolines of tree canopies are slightly expanded compared with the corresponding α -isolines of clear skies, so that the (Arago, Babinet, or Brewster) neutral points can disappear (Fig. 4). Figure 6 shows an example of this phenomenon: Here the α -patterns of the clear sky in scene S7 and the tree canopy in scene S8 measured under the same sky conditions (Table 1) in the blue spectral range are compared with the theoretical patterns calculated on the basis of the single-scattering Rayleigh model and the model of Berry *et al.* [15]. We can see that the α -pattern of the overhead vegetation more closely resembles the Rayleigh pattern than the real (measured) one or the pattern of Berry *et al.* [15].

Finally, we observed that if the overhead vegetation was not sunlit, because the sun was below the horizon (not shown here), or was occluded by clouds (scenes S27, S30, S32 in Fig. 4), then the α -pattern of the foliage was extremely distorted so that there was no trace of mirror symmetry and the noisiness of α was rather large ($37\% \leq n_{\text{foliage}} \leq 43\%$).

4. Discussion and Conclusions

In forests the large-scale spatiotemporal distribution of the radiance, color, and polarization of the ambient light is complex. Different areas receive light directly from the sun and/or the sky and/or indirectly via the leaves. On the basis of the intensity and color of the light field, Endler [12] categorized four major light environments in forests when the sun is not blocked by clouds: “forest shade,” “woodland shade,” “small gaps,” and “large gaps,” characterized by yellow-green, blue-gray, reddish, and white ambient light spectra, respectively. A fifth light environment is associated with low solar elevation angles near dawn

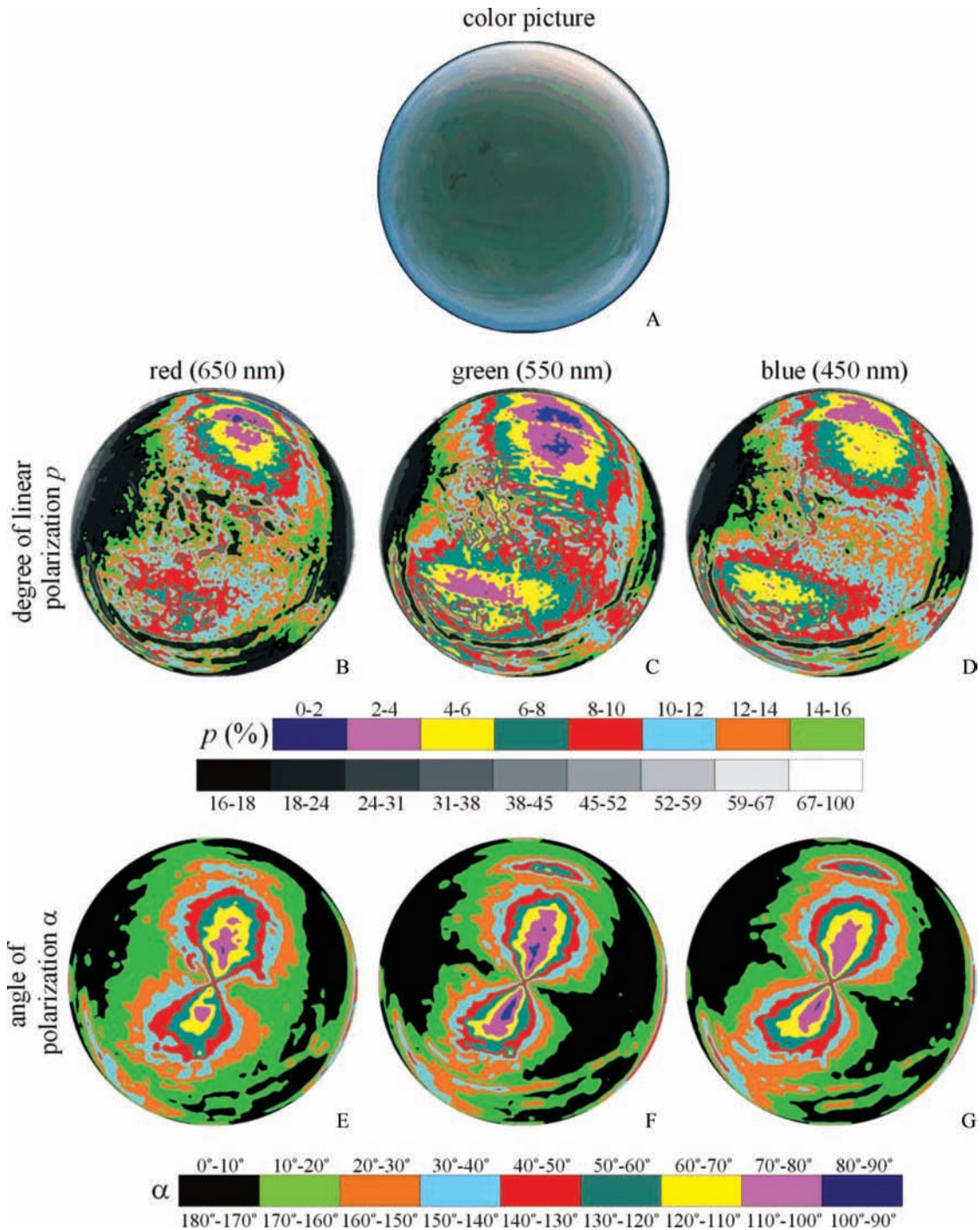


Fig. 2. (Color online) As Fig. 1 for scene S0 with grassland lit by the rising sun. The measurements were performed from a hot air balloon at an altitude of 100 m. The optical axis of the fisheye lens pointed toward the nadir, which is the center of the circular patterns.

and dusk, which is purplish. Shashar *et al.* [10] characterized qualitatively the polarization features of these light fields. Using videopolarimetry, Shashar *et al.* [10] and Horváth *et al.* [11] measured the polarization patterns of some plant leaves. They showed that these polarization patterns are complex, and strongly depend on the surface characteristics of the leaf, the orientation of the leaf blade, and the illumination conditions.

Considering the small-scale optical environment in forests, the surface of leaves (as every dielectric boundary does) reflects, scatters, and transmits the incident light [20]. Polarized light reflected by a leaf contains information on both surface-roughness and orientation of the leaf blade [4–8]. The reflection-polarization characteristics of a leaf depend on the leaf's surface features [9]. Leaf reflectance is intermediate between that of a perfectly diffuse Lambert

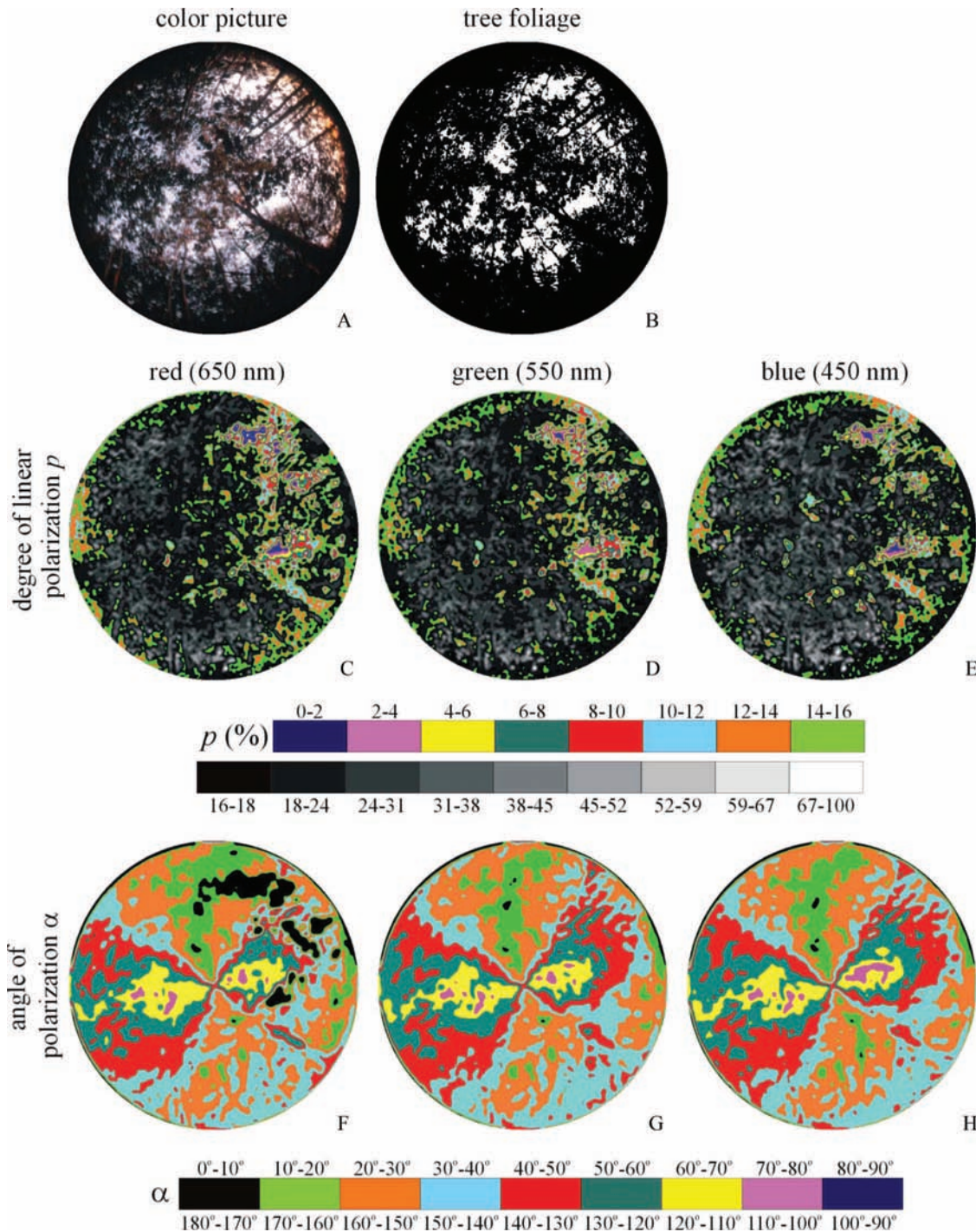


Fig. 3. (Color online) As Fig. 1 for scene S22 with the overhead vegetation of a forest composed of birch trees lit by the setting sun. In pattern B black shows the tree foliage and white indicates the sky.

reflector (reflecting the incident light uniformly into all directions) and a perfectly specular Fresnel reflector (being a smooth interface between two different dielectric media, the polarizing ability of which is described by Fresnel's law of reflection), which suggests that it is the sum of diffuse and specular components [21]. The diffuse component is unpolarized, varies little with changing angles, and its spectrum is characteristic to the (usually green) leaf tissue. The

specular component is partially linearly polarized, is reflected from the outermost leaf surface (cuticle), spreads about the specular direction, and has a spectrum that is practically the same as that of the incident light [9].

The roughness of the leaf surface determines the angular spread of the specularly reflected polarized light. Visibly shiny leaves tend to have higher specular reflectance than matte ones although leaves that

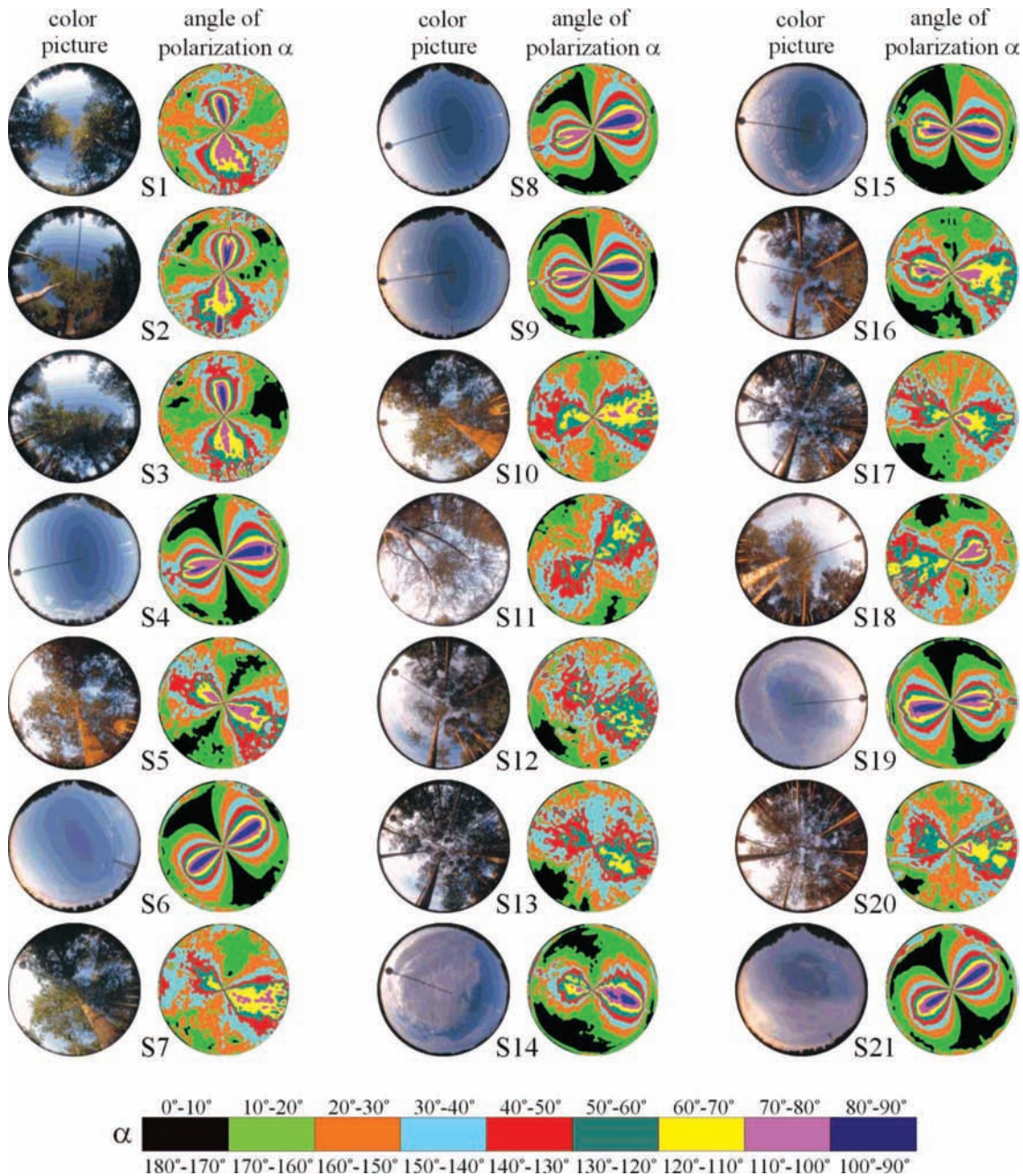


Fig. 4. (Color online) Color pictures and α -patterns of Finnish skies and tree canopies (scenes S1–S42, Tables 1 and 2), measured in the blue part of the spectrum. Quite similar α -patterns were obtained in the green and red spectral ranges.

have no shiny appearance can still specularly reflect light. Leaves with sparsely distributed hairs can specularly reflect more light than glabrous (hair-free) leaves and some highly pubescent (hairy) leaves may be strong specular reflectors [9]. Small particles and features on the leaf surface scatter light away from the specular direction. The polarized reflectance equals the specular reflectance when the angles of incidence and reflectance both equal Brewster's angle, approximately 55° from the normal vector of the wax-coated leaf surface [22].

Let us consider the physical reasons for our finding that the α -pattern of the sunlit foliage is qualitatively

the same as that of the clear sky (Figs. 2–4); i.e., the direction of polarization of light from the sunlit overhead vegetation is approximately perpendicular to the plane determined by the observer, the sun and the leaf observed. Figure 5 shows schematically the nine components (T-SU, T-SK, T-LE, S-SU, S-SK, S-LE, D-SU, D-SK, and D-LE) of the light from the foliage and its polarization characteristics. A particular leaf of the foliage is illuminated by sunlight (SU), and/or skylight (SK), and/or light from the neighboring leaves (i.e., leaflight, LE). SU is unpolarized ($p = 0$), while SK and LE are partially linearly polarized ($p > 0$) due to scattering-polarization and reflection-

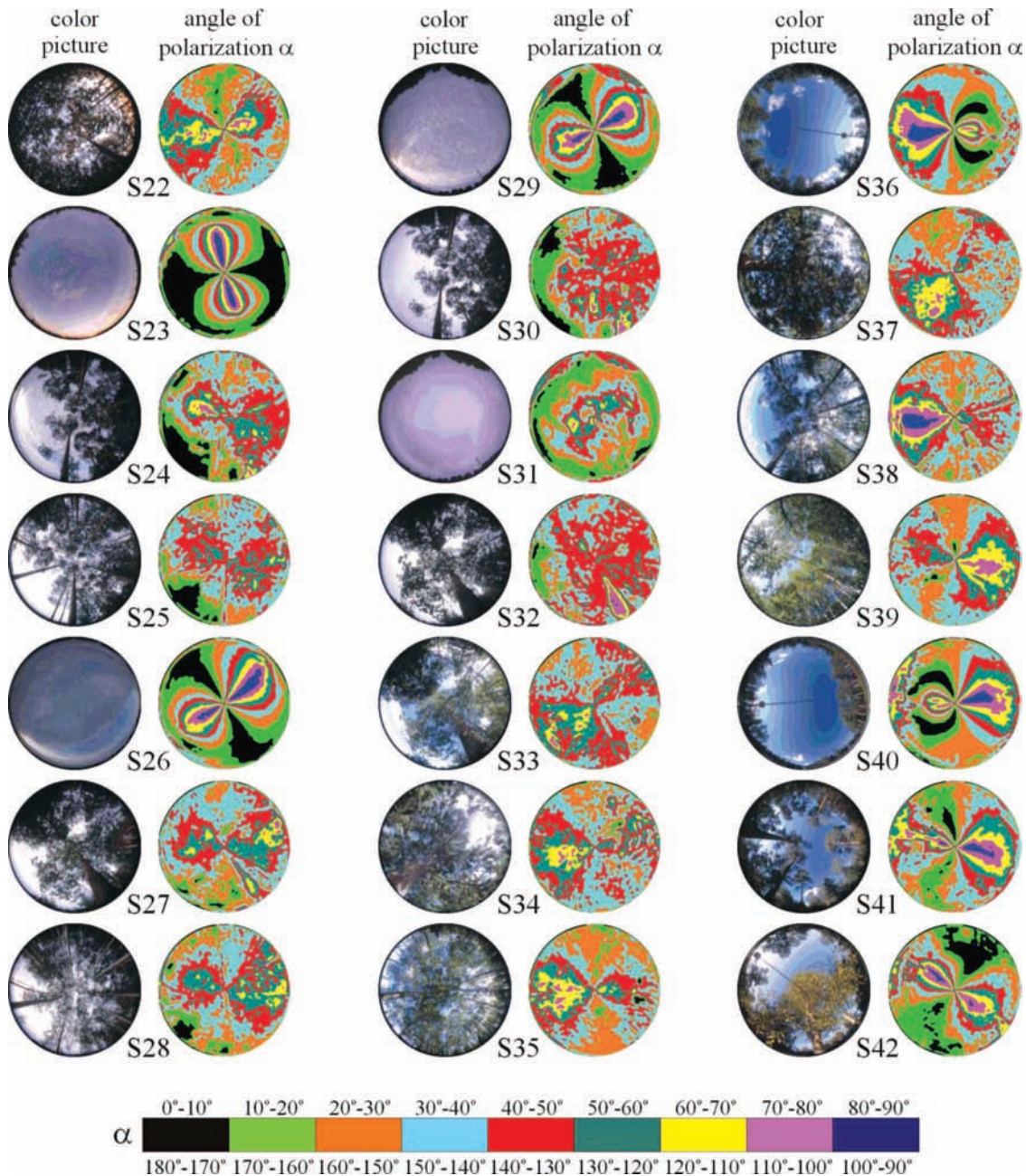


Fig. 4. *Continued.*

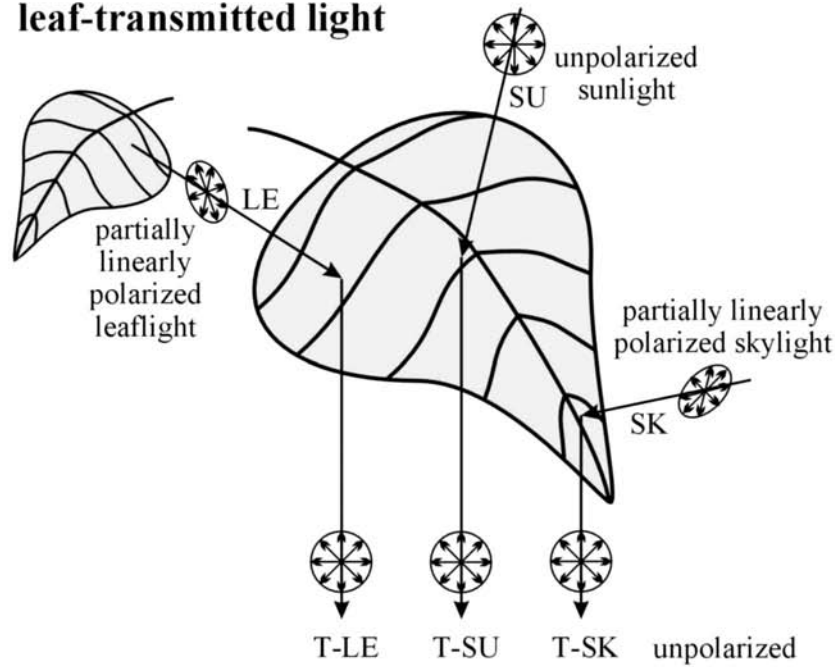
polarization of sunlight in the atmosphere and at the leaf blades, respectively [2,9,11,23]. The leaflight has two main components: light transmitted through the leaves [Fig. 5(A)] and light reflected by the leaves [Fig. 5(B)]. The former possesses three further components: the sunlight (T-SU), skylight (T-SK), and leaflight (T-LE) transmitted through the leaves. T-SU, T-SK and T-LE are practically unpolarized ($p \approx 0$) because of the diffuse scattering and multiple reflection of light (SU, SK, LE) within the leaf tissue [2,9,11,23] [Fig. 5(A)].

Light can be reflected from a leaf either diffusely by the leaf's tissue and its rough outer surface (due to hairs or wax), or specularly from smooth leaf cuticle

[2,9,11] [Fig. 5(B)]. If the incident light (SU, SK, LE) penetrates into the leaf tissue, it can either be diffusely reflected into all directions after multiple scattering on and reflection from the plant cells (D-SU, D-SK, D-LE), or be transmitted diffusely through the leaf (T-SU, T-SK, T-LE). The diffusely reflected components D-SU, D-SK, and D-LE are practically unpolarized ($p \approx 0$) [9,11]. The specularly reflected components S-SU, S-SK, and S-LE are partially linearly polarized [2,9,11,23]. According to Fresnel's laws of reflection [24], the direction of polarization of specularly reflected light is perpendicular to the plane of reflection determined by the incident light, reflected light, and the local normal vector of the

leaf-transmitted light

A



leaf-reflected light

B

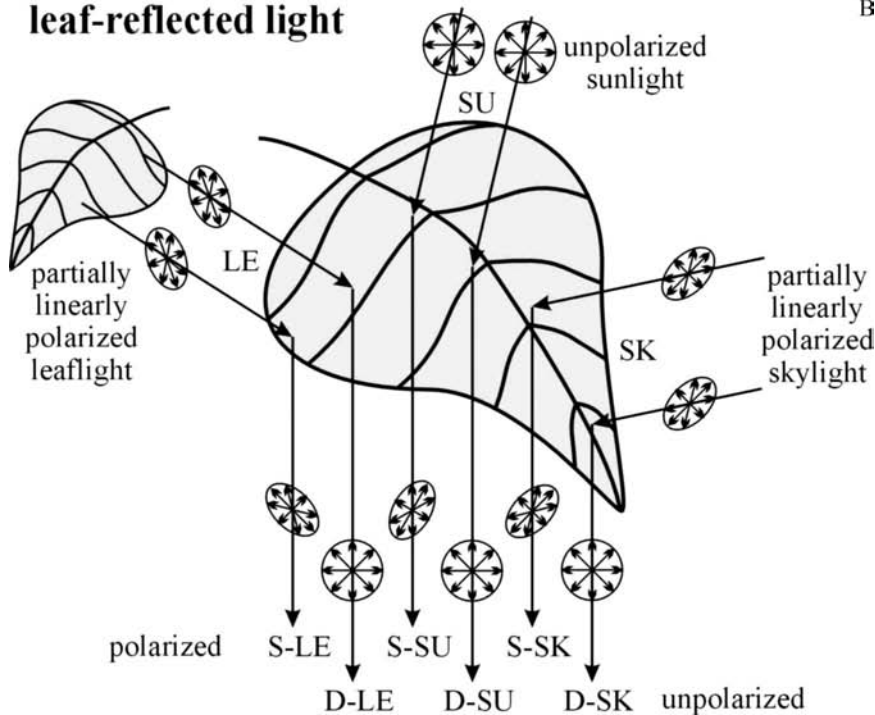


Fig. 5. Schematic representation of the polarization characteristics of the different components (SU, S-SK, S-LE, D-SU, D-SK, D-LE, T-SU, T-SK, T-LE) of light transmitted (A) and reflected (B) by a leaf in the foliage. Circles and ellipses with double-headed arrows represent unpolarized and partially linearly polarized light, respectively. SU: sunlight (unpolarized); SK: skylight (partially linearly polarized); LE: leaflight (partially linearly polarized); S-SU, S-SK and S-LE: specularly reflected sunlight, skylight and leaflight (partially linearly polarized); D-SU, D-SK and D-LE: diffusely reflected sunlight, skylight and leaflight (unpolarized); T-SU, T-SK and T-LE: transmitted sunlight, skylight and leaflight (unpolarized).

reflecting surface. Thus, the direction of polarization of S-SU is perpendicular to the plane containing the observer, the sun, and the observed point of a sunlit leaf. The direction of polarization of the other two specularly reflected components S-SK and S-LE are usually tilted to this plane, because the direction of

the incident skylight (SK) and leaflight (LE) is generally different from that of the sunlight (SU).

From what has been explained above, it follows that among the nine components of leaflight only the sunlight reflected specularly from the smooth cuticle of leaves (S-SU) can result in directions of polariza-

tion perpendicular to the plane of reflection passing through the observer, the sun, and the observed sunlit leaf of the foliage. This S-SU component is the reason for the white gloss of shiny (smooth) sunlit leaves. This highly polarized, cuticle-reflected gloss often overwhelms the unpolarized green light reflected diffusely from the leaf tissue. According to Können [23], in the foliage there can be many leaves oriented in many different directions, but the gloss of the foliage as a whole is tangentially polarized with respect to the sun, i.e., perpendicular to the plane of reflection.

This model also explains why under the same sky conditions the 8-shaped α -isolines of tree canopies expand relative to those of the clear sky, so that the neutral points may disappear: since the S-SU component, per definition, practically corresponds to the single scattering of light, the α -pattern of sunlit overhead vegetation resembles the Rayleigh pattern. The α -pattern of the clear sky more or less deviates from the Rayleigh pattern due to the multiple scattering of light in the air (Fig. 6).

Thus we conclude that if the vegetation is sunlit, then the α -pattern of the foliage is qualitatively the

same (scenes S1–S3, S5, S7, S10–S13, S16–S18, S20, S22, S24, S25, S28, S33–S35, S37–S39, S41, S42 in Fig. 4) as that of the clear sky (Fig. 1, and scenes S4, S6, S8, S9, S15, S36, S40 in Fig. 4). The main reason for this phenomenon is the polarization effect of the S-SU component of leaflight. Consequently, the illumination of the foliage by direct sunlight plays an important role, while solar elevation and sky conditions (clear or partly cloudy with visible sun's disc) are irrelevant. The deviations of the α -pattern of the sunlit vegetation from that of the clear sky are the consequences of the polarization characteristics of the other eight components T-SU, T-SK, T-LE, S-SK, S-LE, D-SU, D-SK, and D-LE of the leaflight. The larger the contribution of these eight components to the net leaflight, the greater these deviations. If the sun is occluded by clouds, the foliage is not sunlit, thus the S-SU component does not exist and consequently the α -pattern of the foliage (scenes S27, S30, S32 in Fig. 4) differs considerably from that of the clear sky (Fig. 1, and scenes S4, S6, S8, S9, S15, S36, S40 in Fig. 4). Physically it is obvious that the same holds true for moonlit scenes at night, when the main

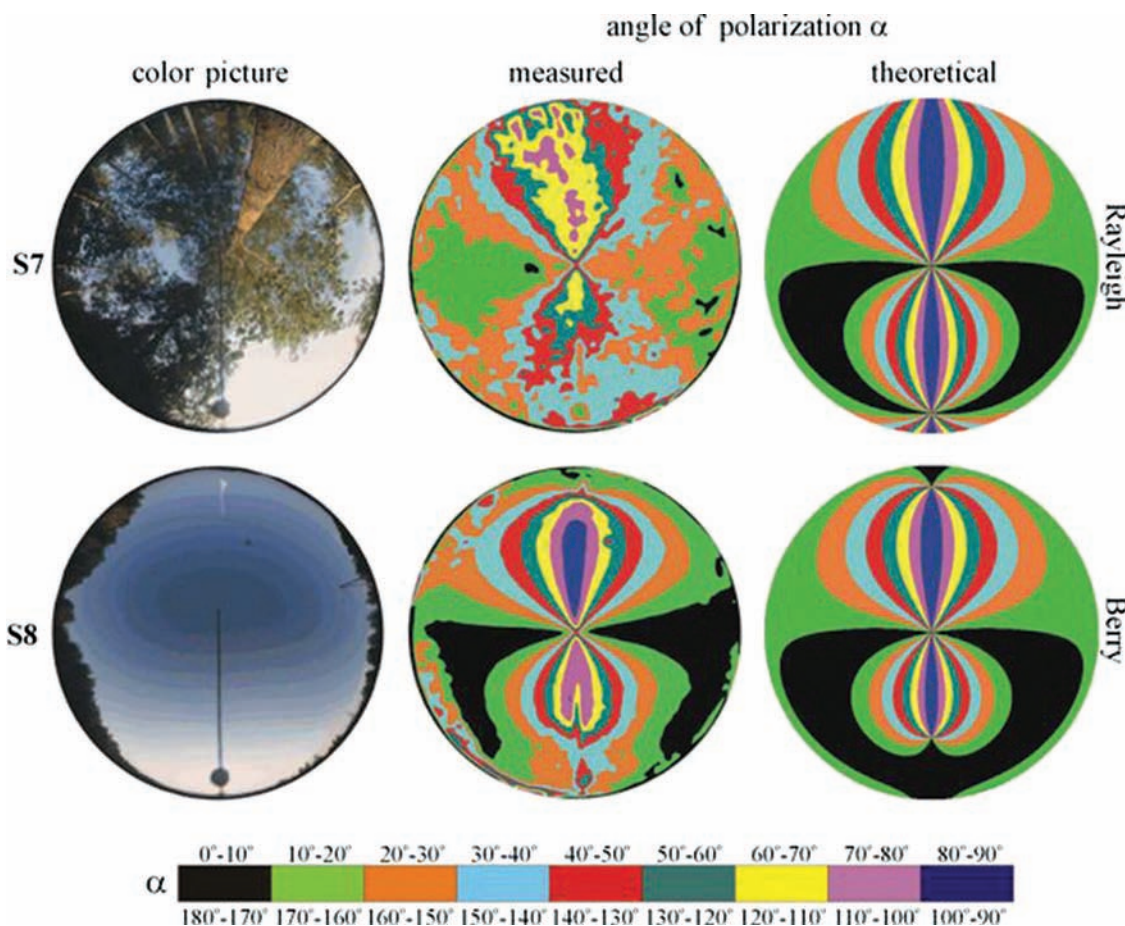


Fig. 6. (Color online) *Left and middle columns*: Color pictures and the α -patterns of a clear sky (scene S7) and the tree canopy (scene S8), measured in the blue (450 nm) part of the spectrum under the same sky conditions (Table 1). *Right column*: Theoretical α -patterns calculated on the basis of the single-scattering Rayleigh-model (for S7) and the model of Berry *et al.* (2004) (for S8), respectively. For the sake of easier comparisons, the circular pictures and patterns were rotated so that the solar-antisolar meridian became vertical in both cases.

source of light is sunlight reflected by the moon, if the latter is not occluded by clouds.

Although our polarimetric measurements happened in calm weather, in wind the leaves are constantly in motion. Due to the wind-generated oscillation of the leaf blades, both p and α of leaflight more or less fluctuate. Under this situation the time-averaged p - and α -values of light from the vegetation possess similar characteristics as shown in Figs. 2–4, 6 and Table 2 measured in calmness.

Earlier it has been shown that the α -pattern of the sky during the full moon at night [25] and during the day under smoky [17], foggy [18], and partly cloudy [3,18,26,27], as well as total overcast conditions [19] is qualitatively the same as that of the clear, sunlit sky. Thus, our full-sky imaging polarimetric results presented here supplement these earlier findings, demonstrating that the distribution of the angle of polarization is a very stable pattern in the optical environment encompassing both sunlit and moonlit skies and including sunlit grassland and overhead vegetation.

According to Shashar *et al.* [10], the polarization of the sky can be determined in rain forests even from beneath the tree canopy and can be used by animals living on the ground or in the lower parts of the forest, as long as they have a clear view of a large portion of the sky. However, we have shown in this work that the α -pattern of sunlit tree canopies is qualitatively the same as that of the clear sky. We conclude that as a consequence of the sky-specific α -pattern underneath sunlit tree canopies, polarization-based navigation in forests is not limited to spaces exposed to several extended portions of the clear sky.

Barta and Horváth [28] were able to show that if the space under the foliage is partly sunlit, p of downwelling light from the overhead vegetation is maximal in the UV, because in this spectral range the unpolarized UV-deficient green leaflight dilutes least the polarized light scattered in the air beneath the foliage. Therefore, in daytime the detection of the polarization of downwelling light under tree canopies is most advantageous in the UV, because in this spectral range the risk that p is lower than the threshold p^* of polarization sensitivity in animals is smallest. On the other hand, Hegedüs *et al.* [29] explained why longer wavelengths are advantageous for the perception of the polarization of downwelling light from overhead vegetation illuminated by the setting sun. Using three atmospheric optical models, they computed the p and the polarized radiance ($= p \cdot I$, where I is the total radiance) of downwelling leaflight, the quantum catch (number of photons absorbed by a photoreceptor), and quantum catch difference between polarization detectors with orthogonally arranged microvilli under foliage illuminated by the setting sun as functions of the wavelength and the solar zenith angle. They showed that using green-sensitive polarization detectors for polarization-based orientation under tree canopies at low solar elevations is an optimal compromise between the simultaneous maximization of the quantum catch

and the quantum catch difference. This explains why dusk-active European cockchafers, *Melolontha melolontha* detect the polarization of downwelling light in the green part of the spectrum. Cockchafers are active at sunset and fly predominantly under the foliage lit by the setting sun during their swarming, feeding, and mating periods. In the retina of *M. melolontha* the polarization of downwelling light (skylight or light from the foliage) is detected by photoreceptors in upward-pointing ommatidia with a maximal sensitivity at 520 nm in the green part of the spectrum. According to Hegedüs *et al.* [29], polarization vision in *M. melolontha* underneath green foliage during sunset is tuned to the high polarized intensity of downwelling light in the green.

Since the mirror symmetry axis of the α -pattern of the sunlit overhead vegetation is always the solar-antisolar meridian, the azimuth direction of the sun occluded by foliage in forests can be assessed from this polarization pattern. (Note that only the solar azimuth, i.e., the direction of the solar meridian can be determined, rather than the solar position, possessing two components: the azimuth and the elevation.) For instance, tropical honey bees (the ancestors of all recent bees), living and dancing on exposed limbs in tropical forests, are frequently confronted with the problem of orientation underneath sunlit overhead vegetation [30]. According to Brines and Gould [3] such bees flying or dancing under a canopy of vegetation might well be able to see perfectly good patterns of polarized UV light against the leaves overhead. In this work we presented polarimetric evidence in favor of this hypothesis for the visible part of the spectrum, based on our finding that the α -pattern of the sunlit foliage in forests is qualitatively the same as that of the clear sky. A further important argument is that during the day the detection of the polarization of downwelling leaflight is most advantageous in the ultraviolet [28], and many day-active insects, such as honey bees (*Apis mellifera*), bumblebees (*Bombus hortorum*), desert ants (*Cataglyphis bicolor*, *C. setipes*), flies (*Calliphora erythrocephala*, *Musca domestica*), scarab beetles (*Lethrus apterus*, *L. inermis*, *Pachysoma striatum*), for instance, perceive the polarization of skylight in the ultraviolet [31].

Thus, the following scenario for the evolution of polarization-based navigation in bees can be imagined: In the ancient bees, living in forests, the ability to perceive downwelling polarized leaflight has evolved in the UV part of the spectrum in order to assess the azimuth direction of the invisible sun (occluded by foliage) from the α -pattern of the sunlit overhead vegetation for navigation purposes. Later, when the descendants of these ancient bees dispersed from the tropical forests into other regions, this ability was used to perceive the polarization of the skylight in the UV even under cloudy conditions in order to determine the azimuth of the sun, hidden by clouds, for the purpose of orientation. According to this hypothesis, the perception of polarized leaflight in forests for navigational reasons, preceded the detection of polarized skylight and use of direct celestial

polarization for orientational purposes. Although this hypothesis cannot be proven, it is logical and strongly supported by the arguments advanced in this paper and our polarimetric results in the field.

Gábor Horváth is grateful to the German Alexander von Humboldt Foundation for an equipment donation, and Victor Benno Meyer-Rochow wishes to acknowledge the support received for this project from Oulu University's Department of Biology. We also very much thank Prof. Rüdiger Wehner (Department of Zoology, University of Zürich, Switzerland) for lending us his Nikon fisheye lens for our polarimetric measurements. Thanks also to two anonymous reviewers for their valuable comments.

References

1. I. A. Kong, *Polarimetric Remote Sensing* (Elsevier, 1990).
2. K. L. Coulson, *Polarization and Intensity of Light in the Atmosphere* (A. Deepak Publishing, 1988).
3. M. L. Brines and J. L. Gould, "Skylight polarization patterns and animal orientation," *J. Exp. Biol.* **96**, 69–91 (1982).
4. V. C. Vanderbilt and L. Grant, "Polarization photometer to measure bidirection reflectance factor $R(55^\circ, 0^\circ, 55^\circ, 180^\circ)$ of leaves," *Opt. Eng.* **25**, 566–571 (1985).
5. V. C. Vanderbilt, L. Grant, and C. S. T. Daughtry, "Polarization of light scattered by vegetation," *Proc. IEEE* **73**, 1012–1024 (1985).
6. V. C. Vanderbilt, L. Grant, L. L. Biehl, and B. F. Robinson, "Specular, diffuse and polarized light scattered by two wheat canopies," *Appl. Opt.* **24**, 2408–2418 (1985).
7. L. Grant, C. S. T. Daughtry, and V. C. Vanderbilt, "Polarized and non-polarized leaf reflectances of *Coleus blumei*," *Environ. Exp. Bot.* **27**, 139–145 (1987).
8. L. Grant, C. S. T. Daughtry, and V. C. Vanderbilt, "Variations in the polarized leaf reflectance of *Sorghum bicolor*," *Remote Sens. Environ.* **27**, 333–339 (1987).
9. L. Grant, C. S. T. Daughtry, and V. C. Vanderbilt, "Polarized and specular reflectance variation with leaf surface features," *Physiol. Plant.* **88**, 1–9 (1993).
10. N. Shashar, T. W. Cronin, L. B. Wolff, and M. A. Condon, "The polarization of light in a tropical rain forest," *Biotropica* **30**, 275–285 (1998).
11. G. Horváth, J. Gál, T. Labhart, and R. Wehner, "Does reflection polarization by plants influence colour perception in insects? Polarimetric measurements applied to a polarization-sensitive model retina of *Papilio* butterflies," *J. Exp. Biol.* **205**, 3281–3298 (2002).
12. J. A. Endler, "The color of light in forests and its implications," *Ecol. Monogr.* **63**, 1–27 (1993).
13. G. Horváth, B. Bernáth, B. Suhai, A. Barta, and R. Wehner, "First observation of the fourth neutral polarization point in the atmosphere," *J. Opt. Soc. Am. A* **19**, 2085–2099 (2002).
14. J. Gál, G. Horváth, V. B. Meyer-Rochow, and R. Wehner, "Polarization patterns of the summer sky and its neutral points measured by full-sky imaging polarimetry in Finnish Lapland north of the Arctic Circle," *Proc. R. Soc. London, Ser. A* **457**, 1385–1399 (2001).
15. M. V. Berry, M. R. Dennis, and R. L. Jr. Lee, "Polarization singularities in the clear sky," *New J. Phys.* **6**, doi: 10.1088/1367-2630/6/1/162 (2004).
16. J. H. Hannay, "Polarization of sky light from a canopy atmosphere," *New J. Phys.* **6**, doi: 10.1088/1367-2630/6/1/197 (2004).
17. R. Hegedüs, S. Åkesson, and G. Horváth, "Anomalous celestial polarization caused by forest fire smoke: why do some insects become visually disoriented under smoky skies?" *Appl. Opt.* **46**, 2717–2726 (2007).
18. R. Hegedüs, S. Åkesson, R. Wehner, and G. Horváth, "Could Vikings have navigated under foggy and cloudy conditions by skylight polarization? On the atmospheric optical prerequisites of polarimetric Viking navigation under foggy and cloudy skies," *Proc. R. Soc. London, Ser. A* **463**, 1081–1095 (2007).
19. R. Hegedüs, S. Åkesson, and G. Horváth, "Polarization patterns of thick clouds: overcast skies have distribution of the angle of polarization similar to that of clear skies," *J. Opt. Soc. Am. A* (in press) (2007).
20. J. T. Woolley, "Reflectance and transmittance of light by leaves," *Plant Physiol.* **47**, 656–662 (1971).
21. L. Grant, "Diffuse and specular characteristics of leaf reflectance," *Remote Sens. Environ.* **22**, 309–322 (1987).
22. V. P. Rvachev and S. G. Guminetskii, "The structure of light beams reflected by plant leaves," *J. Appl. Spectrosc.* **4**, 415–421 (1966).
23. G. P. Können, *Polarized Light in Nature* (Cambridge University Press, 1985).
24. R. M. A. Azzam and N. M. Bashara, *Ellipsometry and Polarized Light* (North-Holland, 1992).
25. J. Gál, G. Horváth, A. Barta, and R. Wehner, "Polarization of the moonlit clear night sky measured by full-sky imaging polarimetry at full moon: comparison of the polarization of moonlit and sunlit skies," *J. Geophys. Res. D* **106**, 22647–22653 (2001).
26. I. Pomozi, G. Horváth, and R. Wehner, "How the clear-sky angle of polarization pattern continues underneath clouds: full-sky measurements and implications for animal orientation," *J. Exp. Biol.* **204**, 2933–2942 (2001).
27. B. Suhai and G. Horváth, "How well does the Rayleigh model describe the E-vector distribution of skylight in clear and cloudy conditions? A full-sky polarimetric study," *J. Opt. Soc. Am. A* **21**, 1669–1676 (2004).
28. A. Barta and G. Horváth, "Why is it advantageous for animals to detect celestial polarization in the ultraviolet? Skylight polarization under clouds and canopies is strongest in the UV," *J. Theor. Biol.* **226**, 429–437 (2004).
29. R. Hegedüs, Á. Horváth, and G. Horváth, "Why do dusk-active cockchafers detect polarization in the green? The polarization vision in *Melolontha melolontha* is tuned to the high polarized intensity of downwelling light under canopies during sunset," *J. Theor. Biol.* **238**, 230–244 (2006).
30. E. O. Wilson, *Insect Societies* (Harvard University Press, 1971).
31. G. Horváth and D. Varjú, *Polarized Light in Animal Vision—Polarization Patterns in Nature* (Springer-Verlag, 2003).